

Design Study for a Laminar-Flying-Wing Aircraft*

T. I. Saeed[†] and W. R. Graham[‡]

University of Cambridge, Cambridge, CB2 1PZ, UK

The Greener by Design initiative has identified the laminar-flying-wing configuration as the most promising long-term prospect for fuel-efficient civil aviation. However, in the absence of detailed evaluations, its potential remains uncertain. As an initial contribution, this work presents a point design study for a specification chosen to maximize aerodynamic efficiency, via large wingspan and low sweepback. The resulting aircraft carries 220 passengers over a range of 9000km at Mach 0.67, and has a lift-to-drag ratio of 60.9, far in excess of conventional passenger transports. However, its overall effectiveness is compromised by a high empty-to-payload weight ratio and, due to the huge discrepancy between cruise and climb-out thrust requirements, a poor engine efficiency. As a result, it has a much less marked fuel-consumption advantage (11.4–13.9g per passenger kilometer, compared to 14.6) over a conventional competitor designed, using the same methods, for the same mission. Both weight ratio and engine efficiency could be improved by reducing aspect ratio, but at the cost of an aerodynamic efficiency penalty. This conflict, which has not previously been recognized, is inherent to the laminar-flying-wing concept, and may undermine its attractiveness.

*An earlier version of this paper, AIAA 2012-0868, was presented at the 50th AIAA Aerospace Sciences Meeting, Nashville, TN.

[†]Research Student, Department of Engineering. Current post: Research Associate, Department of Aeronautics, Imperial College, London.

[‡]Senior Lecturer, Department of Engineering, Member AIAA.

Nomenclature

A_R	=	wing aspect ratio
C_D	=	aircraft drag coefficient
C_{D_i}	=	induced-drag coefficient
C_{D_v}	=	viscous-drag coefficient
C_{D_0}	=	zero-lift-drag coefficient
C_L	=	aircraft lift coefficient
C_l	=	airfoil section lift coefficient
C_p	=	pressure coefficient
c	=	local wing chord
c_{ref}	=	reference wing chord
D	=	aircraft drag
e	=	Oswald efficiency, $C_L^2/\pi A_R C_{D_i}$
F_N	=	engine thrust
H_0	=	fuel (lower) calorific value
L	=	aircraft lift
M_∞	=	flight Mach number
s	=	specific fuel consumption
U_∞	=	flight speed
W_e	=	aircraft empty weight
W_f	=	fuel weight
W_p	=	payload weight
W_X	=	engine power off-take
x	=	airfoil section horizontal coordinate
X	=	range
y	=	airfoil section vertical coordinate, <i>or</i> aircraft spanwise coordinate
η	=	engine overall efficiency

I. Introduction

Civil aviation is under continued pressure to reduce its environmental impact. One of a number of responses to this pressure has been the formation, by the Royal Aeronautical

Society and the UK aerospace industry, of the ‘Air Travel – Greener by Design’ initiative. In a high-level analysis of possible future aircraft configurations,¹ its technology sub-group identified the laminar-flying-wing (LFW) type as the most promising long-term option, estimating its payload fuel efficiency (at current technology levels) as 0.063–0.072g per (payload) kg kilometer. If achievable, this performance would represent a huge improvement on today’s aircraft. (The Greener-by-Design estimate for the payload fuel efficiency of the conventional configuration is 0.148–0.181g per kg kilometer, depending on range; even these values may be optimistic in the light of a quoted consumption of 23.5g per passenger kilometer for the Boeing 777.²)

The promise of the LFW configuration arises from its exceptionally low skin-friction drag, achieved via suction-controlled boundary-layer laminarization. To take full advantage of this feature, the vast majority of the wetted area must be laminarized, and it is generally agreed that this requirement precludes a conventional fuselage. Hence the aircraft must be a pure flying wing. Such a radical concept has not been studied in any detail since the Handley Page HP117 proposal.^a That analysis was based on turbojet propulsion, and predicted a fuel consumption of 22g per passenger kilometer, unremarkable by today’s standards. Further, up-to-date, studies are clearly necessary to test the validity of the Greener-by-Design estimate.

First it must be acknowledged that, while LFC is proven in principle, its application remains subject to practical difficulties.³ Surface finish requirements are demanding, and environmental contamination is a major problem. However, concern over operational issues seems necessary only if the LFW can first be shown to hold sufficient promise to justify its radical nature.

Ultimately, such a demonstration requires a design optimization covering the entire available parameter space. As a starting point, it is desirable to establish realistic boundaries, particularly if they can be identified using simpler analysis methods than required for the general case. The obvious simplification for the LFW is to limit sweepback, so that boundary-layer cross-flow instability analysis is not needed.⁴ This restriction is consistent with a high-aspect-ratio planform, which is necessary if the aerodynamic benefits of laminar flow control are to be fully realized. It is thus possible to explore the parameter-space limit corresponding to pursuit of the best possible lift-to-drag ratio, ahead of structural and propulsion concerns. This is the topic of the present work.

The layout of the paper is as follows. First the methodology is set out. Then the resulting LFW design is summarized. Next, for comparison purposes, a conventional-configuration competitor is proposed. Finally, the implications of the study are discussed. Space limita-

^aG.H. Lee, *All-Wing Laminar Aircraft, Part 2: The HP117 Proposal*. (Unpublished Handley Page report, 1961.)

tions preclude an exhaustive presentation of the aircraft designs; further details can be found in Ref. 5.

II. Design Approach

A. Specification

Normally, an aircraft design begins with a perceived market need, which then defines a mission (i.e. range, speed, payload). Here, in contrast, the starting point is the chosen configuration and the mission is flexible. An initial specification was derived via a high-level analysis of a simplified, constant-chord and constant-sweep, planform. This is set out in full in Chap. 5 of Ref. 5. Briefly, it starts by fixing maximum thickness (as low as possible, limited by a standing-room requirement), sweep angle (as high as possible for stability, subject to boundary-layer cross-flow and attachment-line transition limits), and Mach number (as high as possible without supercritical airfoil flow). Three variable parameters — maximum thickness-to-chord ratio, unit Reynolds number, and span — are then set. This is sufficient to specify cruise conditions (at maximum lift-to-drag ratio), wing loading, and the associated aircraft weight. Due to the remarkably low zero-lift drag predicted with boundary-layer laminarization, maximum L/D is attained at unusually small lift coefficients. The wing loading is correspondingly low, raising the specter of an excessive structural weight fraction. It can be improved by increases in the variable parameters, but these are constrained by their detrimental effects on: cruise Mach number, cabin area and attachment-line transition (for maximum thickness-to-chord ratio), surface-finish requirements and attachment-line transition (unit Reynolds number), and structure weight (span). The compromise values chosen, and the associated design specification, are set out in Tab. 1.

No range or passenger capacity is included in the specification; these parameters were left to be evaluated as part of the subsequent design analysis. However, it has since been found that the unconstrained range would be impractically high, given the cruise Mach number. Therefore this parameter is here set to the figure assumed by Green:¹ 9000km.

B. Methodology

A conventional design algorithm (based on Raymer's prescription⁶) is as follows. First, a suitable donor aircraft, on which to base initial estimates of target weight, surface areas, *etc.*, is identified. The process is then iterative:

- a) target gross weight specified;
- b) cruise lift coefficient estimated, thereby fixing cruise altitude;

Table 1. Laminar-flying-wing aircraft design specification.

Parameter	Value
Maximum thickness (m)	2.5
Thickness-to-chord ratio	0.20
Span (m)	80
Unit Reynolds number (m^{-1})	8×10^6
Sweep (degrees)	25
Chord (m)	12.5
Planform area (m^2)	1000
Aspect ratio	6.4
Cruise lift coefficient	0.14
Mach number	0.67
Altitude (ft)	22500
Velocity (m/s)	209
Allowable weight (kg)	187×10^3
Wing loading (N/m^2)	1835

- c) tailplane geometry defined for balance and stability;
- d) drag assessed in the en-route configuration to provide an estimate of the lift-to-drag ratio;
- e) engine sized;
- f) fuel weight to complete mission calculated;
- g) aircraft structural weight estimated;
- h) maximum take-off weight evaluated and compared with initial target specification.

This is the procedure followed for the competitor aircraft design.

For the LFW, there is no suitable donor aircraft. Instead, the starting point is the specification given in Tab. 1. The design algorithm is then:

- a) detail planform geometry specified to meet comfort and stability requirements;
- b) airfoil sections designed, thereby fixing passenger capacity;
- c) control surfaces specified;
- d) drag assessments carried out for lift-to-drag ratio at key flight conditions;
- e) suction system laid out and power requirements estimated;

- f) engine sized;
- g) fuel weight to complete mission calculated;
- h) aircraft structural weight estimated;
- i) maximum take-off weight evaluated and compared with initial target specification.

III. Analysis Methods

This section describes the main analysis tools employed in the design of the LFW and competitor aircraft. Detail methods for specific instances are referenced where they arise.

A. Aerodynamics

Aerodynamic characteristics are evaluated via quasi-3D analyses. Planform loading distributions and induced drag are calculated with AVL 3.26,^b a vortex-lattice method that also provides any stability derivatives required. Surface pressure distributions are then derived from inviscid compressible-potential-flow computations⁷ in the plane normal to the leading edge. The associated velocities are resolved back into the free-stream direction (as described in Ref. 5) for the boundary-layer calculation, which is an implementation of the Eppler & Somers method⁸ combined with an algorithm for setting suction levels.⁹

In the absence of suction, and especially at low speeds and high lift coefficients, the surface pressures are expected to be affected by boundary-layer growth. For such cases, the coupled panel-method/integral-boundary-layer solver XFOIL¹⁰ is employed.

Section drag is, in general, estimated on the basis of the boundary-layer momentum thickness and shape factor at the trailing edge, via the Squire-Young formula.¹¹ However, this expression applies only for sharp trailing edges. For blunt-ended sections, the trailing-edge momentum thickness is used directly; this approach is conservative, as it neglects the subsequent reduction in momentum thickness due to pressure recovery in the wake. The overall wing drag follows from the integrated section drag contributions.

B. Engine

Propulsion system design is conducted using GasTurb,^c a commercial program which performs a thermodynamic analysis to specify the engine at the chosen design point, and then assesses off-design conditions. The software includes a default set of engine component perfor-

^b<http://web.mit.edu/drela/Public/web/avl/>

^c<http://www.gasturb.de>

mance maps obtained from public-domain data; these were used for all cases. Suction-pump work requirements are accounted for explicitly, via the engine power off-take value.

GasTurb provides a figure for engine weight, but warns that it is likely to be an underestimate. Thus, here, weight is instead obtained from direct scaling of known values for comparable existing engines.

C. Structure

The methodologies presented in Refs. 12 and 13 provide a framework for the structural analysis. Primary elements were sized on the basis of their loading, using preliminary design methods set out by Howe¹⁴ and Greitzer *et al.*¹² Additional component weights were estimated on the basis of empirical correlations with primary element weights.¹⁴ Further detail is provided in Ref. 5.

D. Fuel

The mission fuel consists of climb and cruise components. In addition, the aircraft must carry reserves in case of a diversion, and allowance must be made for unusable fuel.

The climb fuel is calculated as $\Delta E/\eta H_0$, where ΔE is the change in kinetic and potential energies between take-off and maximum altitude. The engine efficiency is set (conservatively) to its value in cruise for the LFW, and at top-of-climb for the competitor aircraft.

The remaining mission fuel is calculated by applying the range equation¹⁵ over the entire flight distance (including climb and descent). For the LFW, cruise (without suction) values for lift-to-drag ratio, velocity, and specific fuel consumption are assumed over flight phases below an altitude of 15,000ft, above which suction is initiated.

Reserve fuel is specified such that the aircraft can fly 200nm and hold for a further 0.75hrs at the cruise fuel-burn rate in the event of a diversion.¹⁶ The unusable fuel is taken as 1% of the sum of mission and reserve fuel.

IV. Laminar Flying Wing Design

This section summarizes the key features of the LFW design. Three flight phases are considered: cruise, cruise without suction (in case of system failure), and climb-out (without suction, which is only applied at an altitude free of dust, insects, *etc.*). The flight speed for the latter is set with reference to conventional aircraft. A Boeing 737-200 in take-off configuration has a stall speed of 63.7m/s,^d which corresponds⁶ to a safe take-off speed of 70m/s. This figure is thus used for the climb-out phase.

^dwww.b737.org.uk/techspecs/detailed.htm

A. Planform

The crude, constant-chord, planform representation of Tab. 1 requires refinement for a realistic design. The leading-edge sweep and overall span will remain fixed at 25° and 80m respectively, but the trailing-edge line will be modified to fulfill comfort, capacity and stability requirements. For the former, Pratt¹⁷ quotes a maximum acceptable passenger acceleration of 0.05g. The latter are obtained from MIL-F-8785C,¹⁸ which denotes the LFW as a *Class III* aircraft. The relevant flight phases are categories B and C; *Level 3* flying qualities are required. A key concern is the longitudinal-static-stability requirement for the neutral point to be aft of the center of gravity (CG), which is often hard to achieve for tailless aircraft.^{19–21}

1. Centerbody

The central part of the LFW contains the passenger cabin, and its width is constrained by the maximum acceptable passenger acceleration during a roll maneuver. MIL-F-8785C specifies that a bank angle of 30° should be achievable in 5s. Given this information, and the roll-subsidence mode time constant, the peak angular acceleration (and hence the centerbody width limit) follow from the standard, single-degree-of-freedom, result for the response to a step aileron input.²² Larger time constants are associated with lower peak accelerations, but require greater aileron moment capability.

The centerbody width limit corresponding to the natural time constant of the LFW was found to be impractically small. Therefore, the peak roll acceleration needs to be artificially limited by the flight control system. Assuming that a conventional roll response is mimicked, a time constant of 4.5s and a slightly relaxed acceleration limit of 0.06g allow the passenger cabin to extend 10m either side of the center-line.

The resulting passenger capacity can be improved by unsweeping the trailing edge of the centerbody, so that its chord increases from 12.5m at its outer limit to 17.2m on the aircraft axis. This also has the beneficial effect of reducing the section thickness-to-chord ratio in the region where isobar unsweep might otherwise lead to shock-wave formation.

2. Outer Wings and Fins

For the sake of an aftwards neutral point, the wing-tip chord and fin height should be maximized. Excessive outboard area would, however, compromise aerodynamic and structural efficiency, so values of 11.3m and 3.5m were chosen, placing the neutral point 11.4m aft of the nose.

Lateral and directional static stability conditions²² were also checked as part of the study. The former is always satisfied; the latter is only breached for CG locations beyond 18m aft. Thus, as expected, the longitudinal-static-stability requirement is the critical one.

3. Planform Summary

The final planform design is shown in Fig. 2(a). The overall area (including fins) is 1088m², with a mean chord of 12.5m. The centerbody has a half-span of 10m and a quarter-chord sweep angle of 19.3°. The outboard quarter-chord sweep is 24.5°.

The neutral-point locations at three flight conditions — cruise with suction applied, cruise without suction, and climb-out — are detailed in Tab. 2. There is a very slight Mach number dependency. Also given are the static-margin values corresponding to the CG locations presented in Sec. H4. The aircraft is close to neutral static stability over all flight phases of interest. In the light of Bolsunovsky *et al.*'s²³ and Northrop's²⁰ suggestions that 3–10% static instability is tolerable for flying-wing aircraft, the design should exhibit satisfactory stability characteristics.

Table 2. Static stability parameters. (CG locations: 11.38m in climb-out and at start of cruise; 11.44m at end of cruise.)

Parameter	Cruise (with suction)	Cruise (no suction)	Climb-out
Flight Mach number	0.67	0.39	0.21
Neutral-point position (m)	11.38	11.41	11.43
Static margin (% c_{ref})	0/-0.5	0.2/-0.2	0.4

B. Airfoil Sections and Cabin Layout

Bespoke airfoil sections were designed manually, with the aid of a section generator written for this purpose. Once a section meeting all local geometrical constraints was identified, the surface pressure distribution at cruise was checked to ensure subcritical flow. This was followed by a boundary-layer calculation, and then a viscous XFOIL analysis at climb-out conditions. In the absence of both supercritical flow and boundary-layer separation the section was accepted; otherwise the design was iterated.

Outboard of the centerbody, the geometrical constraints consist solely of the thickness-to-chord ratio and the wing-spar positions. Inboard, the passenger cabin, a multi-bubble pressure vessel (see Sec. H1) must also be accommodated. The bubble dimensions were chosen to give a minimum cabin height of 1.9m and a seat pitch (at one row per bubble) in excess of the typical 80–90cm,¹⁵ while not breaching the outer envelope of the centerbody. This led to a diameter of 2.14m, with an associated pitch of 1m.

Figure 1 shows a cross-section of a representative multi-bubble cabin embedded within a centerbody wing section. Markers are placed at the front and rear bubble locations to denote minimum clearance requirements for the placement of suction hardware components

and structural elements. Due to the swept leading edge, the forward requirement cannot be met across the entire centerbody span, so the number of bubbles reduces outboard. Adverse pressure gradients associated with the rapid thickness decrease behind the cabin are mitigated via a blunt trailing edge; it is envisaged that the suction air would be discharged in this region.

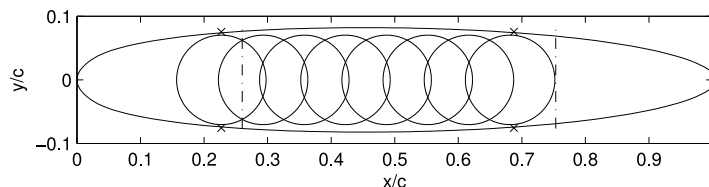


Figure 1. Cross section of the multi-bubble cabin embedded within an airfoil section. Vertical spars located at dash-dot lines; minimum spacings between cabin and wing surface indicated by ‘x’ markers.

Figure 2 details the final airfoil and multi-bubble section geometries, and their associated pressure distributions. Moving out across the centerbody, the (non-dimensional) rear-spar location moves forwards as the chord drops, permitting a lower trailing-edge thickness. In the outboard region, there is no need to maintain high section thickness so far aft, and a sharp trailing edge can be employed. The fins are thinner than the wings, as greater thickness confers no significant structural benefit, and could lead to supercritical flow in the junction region. Their sections are derived from the outer-wing airfoils, scaled down to a thickness-to-chord ratio of 0.1.

This layout provides a total cabin floor area of 138m^2 , of which approximately 7m^2 is required for wardrobes, toilets, *etc.*¹⁵ Taking widths of 0.425m and 0.508m for seats and aisles respectively,¹⁵ and allowing for one aisle per three seats, a passenger capacity of 220 is obtained.

C. Control Surfaces

The control surfaces consist of elevons occupying the outer 67% of wingspan, and rudders on the fins. They are sized on the basis of the low-speed, climb-out, condition, when they are least effective; this is also when the longitudinal static margin is greatest.

Sufficient authority to meet the requirements for pitch trim, roll response (Sec. A1) and engine-out climb (Sec. F1) is provided by 10%-chord surfaces, with the entire elevon span used for pitch control and its outer half for roll. Suction is not applied in these regions. Attached flow is maintained at all settings.

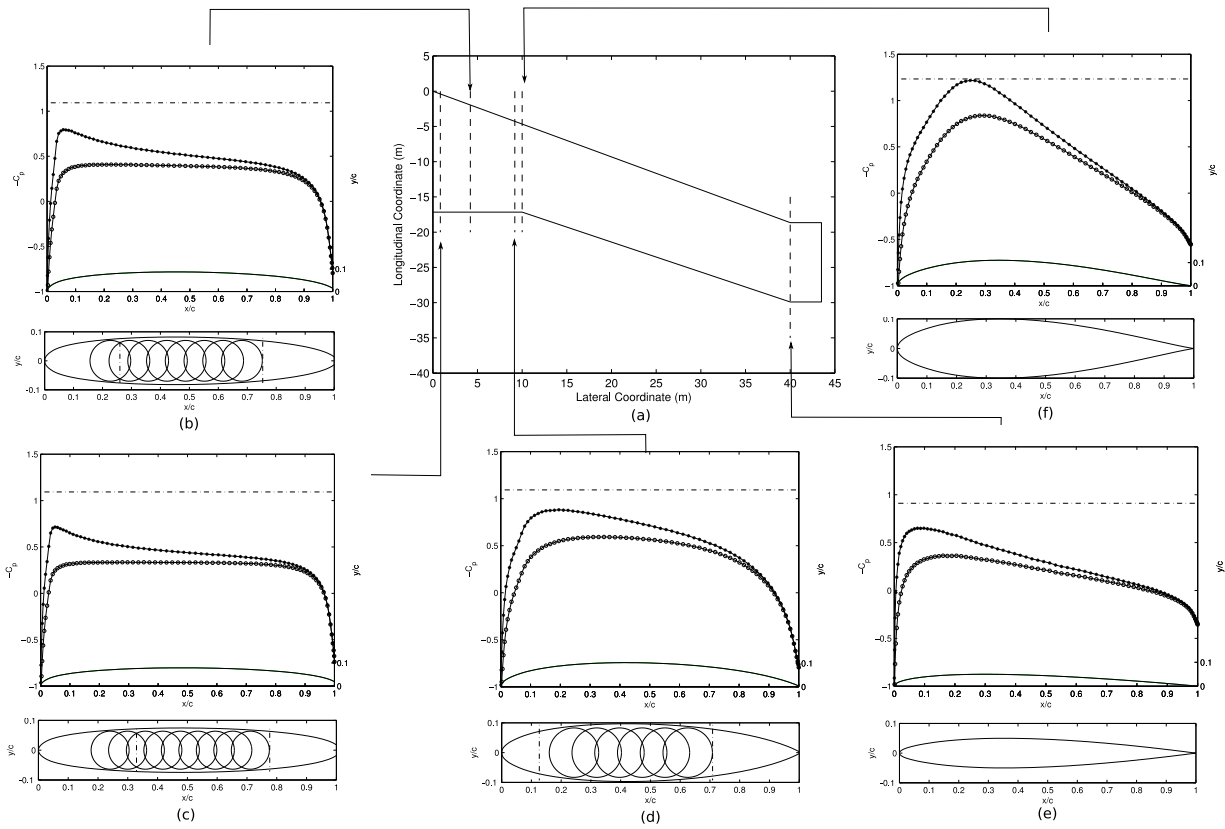


Figure 2. Wing geometry: (a) planform; (b)–(f) selected cross sections showing airfoil, multi-bubble cabin arrangement, and pressure distribution at cruise (with suction). Dash-dot lines indicate sonic pressure coefficients.

D. Performance

1. Cruise Performance with Suction

The combination of symmetrical wing sections, near-neutral stability, and low thrust requirement translates to an elevon deflection of 0.1° upwards for trim. The incidence is 1.5° , which is below the recommended fuselage maximum of 3° .¹⁶ The lift-coefficient distribution is shown in Fig. 3. A favorable value of Oswald efficiency, 1.080, is attained thanks to the efficient all-lifting wing and wingtip-fin combination, and the minimal trim requirement.

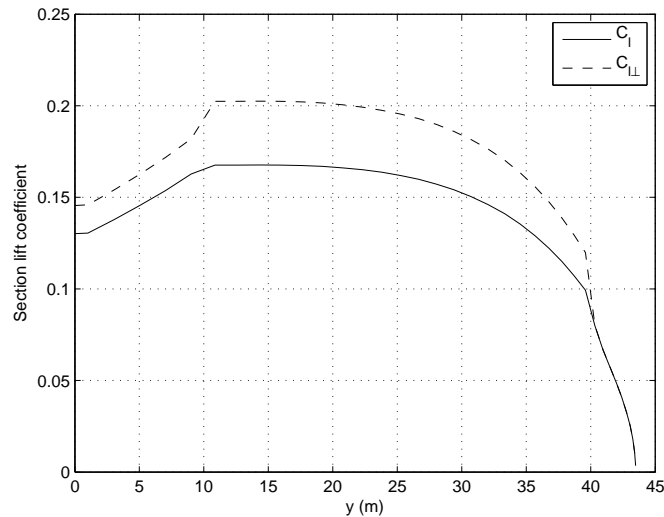


Figure 3. Spanwise variation in section lift coefficient in the free-stream and wing normal directions — $C_L = 0.14$ and $M_\infty = 0.67$.

A drag breakdown is provided in Tab. 3. The miscellaneous viscous drag coefficient consists of contributions from control surface discontinuities,¹⁵ and from engine pylons/nacelles. For the latter, Raymer’s equivalent skin-friction method⁶ was used, assuming: turbulent flow; 10% thick pylons of height 2m and chord 3.5m; 2m diameter nacelles of length 3.5m. The calculated lift-to-drag ratio is 60.9. This figure is significantly higher than current, turbulent, jet-aircraft values of 15–20.²⁴

2. Cruise Performance without Suction

In the event of a suction-system failure, the loss of laminar flow results in a significant increase in total viscous drag. Continuing to fly at the design cruise lift coefficient is far from the optimum, which is proportional to $\sqrt{C_{D0}}$.²⁵ Therefore, cruise C_L is revised, according to this relation, becoming 0.38. Assuming no change in cruise altitude, the corresponding Mach number is 0.39. With a higher thrust requirement, an elevator deflection of 0.8° upwards

is required to trim the aircraft, whilst the incidence goes up to 4.8° . The Oswald efficiency remains unchanged at 1.08, but both induced and viscous drag increase substantially. The lift-to-drag ratio is thus significantly degraded, at 24.8.

3. Climb-Out Performance

The low wing loading means that no high-lift devices are needed to achieve the required lift coefficient. An increase in elevon deflection to 2.5° upwards has a slight beneficial influence on Oswald efficiency, which rises to 1.09. The lift-to-drag ratio is comparable to that in cruise without suction, at 22.4.

Table 3. LFW aerodynamic coefficients.

Coefficient	Cruise	Cruise (no suction)	Climb-out
C_L	0.14	0.38	0.61
C_D	0.0023	0.01535	0.02721
C_{D_i} (e)	0.00098 (1.08)	0.0072 (1.08)	0.01838 (1.09)
C_{D_v} wing	0.00067	0.0075	0.0080
C_{D_v} misc.	0.00065	0.00065	0.00083
L/D	60.9	24.8	22.4

E. Suction System

1. Architecture

The suction-system architecture is based on the arrangement proposed by Saeed *et al.*,⁹ with a series of spanwise chambers at (almost) constant pressure discharging into chord-wise collector ducts for the suction pumps. Saeed *et al.* also presented an algorithm for chamber specification to ensure that avoidable system losses are minimized. This approach was followed without modification for the outer wing, leading to a design consisting of eight upper-surface, and six lower-surface, chambers, with depths set at 0.1m to avoid excessive spanwise pressure losses. The thinner wing-tip fins impose weaker requirements, which are satisfied by six (four) suction- (pressure-) surface chambers, feeding into the wing chambers through throttle valves. The collector ducts and pumps are located at the junctions between the outer wings and the centerbody.

On the centerbody, rapid variations in surface pressure (due to the changes in section thickness-to-chord ratio) render a single continuous-chamber design unworkable. Instead, the arrangement is divided across three regions, as detailed schematically in Fig. 4. Flow-rate controllers throttle the flow between chambers, and the outboard set feed into the pump

collector ducts. The configuration shown is for the upper surface; on the lower, there are two, two and four chambers. The relatively short spanwise extent of the chambers reduces the depth necessary to 0.03m, allowing them to be successfully accommodated in the constrained space between the passenger cabin and the centerbody skin.

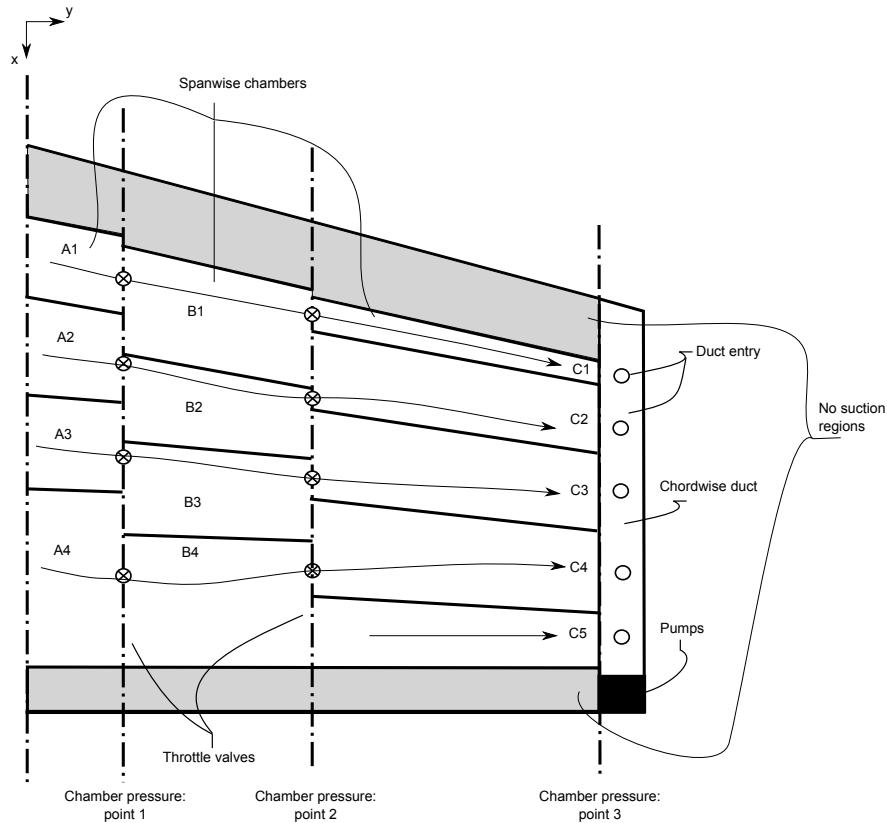


Figure 4. Centerbody suction-system architecture (upper surface).

As noted in Sec. B, the suction flow is to be discharged through the blunt centerbody trailing edge. Pump power requirements are calculated on the basis that the discharge is at flight velocity.

2. Power Requirement and Weight

The calculated suction mass flow at cruise is 43.5kg/s. At an assumed pump efficiency of 85%, the power consumption of the system is 1.87MW. In dimensionless terms,⁹ these figures correspond to a suction coefficient of 3.1×10^{-4} and a power coefficient of 6.3×10^{-4} .

Suction pump weight is estimated from Wilson's²⁶ empirical figure of 0.48kg/kW, which gives 895kg. The spanwise chambers are integrated within the aircraft structure, and are therefore accounted for in Sec. H.

F. Propulsion System

Preliminary investigations revealed that, at the relatively low cruise Mach number of 0.67, turboprop engines offer efficiency benefits over turbofans. A two-spool turboprop architecture, with power off-take from the high-pressure shaft, was therefore adopted. The initial studies also showed that three such engines are required to meet thrust requirements at climb-out.

1. Thrust and Power Requirements

A minimum flight-path angle of 1.55° is required for a three-engined aircraft in climb-out with one engine inoperative.²⁵ At top-of-climb, an ascent-rate of 300 feet per minute must be achievable;²⁵ this translates to a flight-path angle of around 0.5° . In cruise, the flight-path angle is taken to be zero.

Begin- and end-cruise conditions are calculated for a constant-Mach-number cruise climb. This entails a change in Reynolds number. The effect of this change on lift-to-drag ratio is assumed to be negligible. However, its influence on the suction power requirement is accounted for, via the scaling observed by Saeed *et al.*⁹ This translates to an increase of just under 7%. Also included in the power off-take is an auxiliary power requirement of 50kW (the default value within GasTurb).

Table 4 summarizes the requirements per engine over a range of flight conditions. The obvious design challenge is that only around one-seventh of the climb-out thrust is needed for cruise with suction.

Table 4. Thrust and power off-take requirements (per engine) at various flight conditions.

Parameter	Suction			No suction		
	Top of climb	Begin cruise	End cruise	Begin cruise	End cruise	Two-engine climb-out
Altitude (m)	6858	6858	8717	6858	8137	120
Mach number	0.67	0.67	0.67	0.39	0.39	0.21
Thrust (kN)	15.4	10	8.4	24.7	20.7	65.7
Power off-take (kW)	672	672	715	50	50	50

2. Design Approach

Aircraft engines sized for conditions at top-of-climb normally provide ample thrust at take-off.²⁴ In contrast, the study for the (turbojet-powered) HP117 found that, with a large difference in thrust requirement between climb-out and cruise, the former was more critical. This is also the case here, so climb-out had to be adopted as the engine design point. Hence

the default design-point locations on the component performance maps provided by GasTurb were, in some cases, unsuitable, and required alteration.

In addition to the requirements imposed by the airframe, the following design parameters were specified: fuel lower calorific value 43.1MJ/kg (kerosene); compressor and burner exit temperature limits 900K and 1800K respectively; propellor diameter 4.15m; propellor speed 1150RPM. The temperature limits are representative of current technology levels,²⁴ while the propellor size and rotation rate were chosen to avoid excessive values of tip speed,²⁷ thrust coefficient and power coefficient.¹⁵

3. Engine Performance

The calculated engine performance is summarized in Tab. 5. The specific fuel consumption, s , is the rate of fuel use per unit thrust, and is the conventional figure of merit for a turbofan engine. Of more fundamental significance is the overall efficiency of the propulsion system, i.e. the ratio of output work to fuel energy consumed. This can be written in terms of the specific fuel consumption as follows:

$$\eta = \frac{U_\infty + W_X/F_N}{sH_0}. \quad (1)$$

(Note that the standard form of this expression has been extended to include power off-take in the useful work.) Its values are also included in Tab. 5.

Table 5. LFW engine performance.

Parameter	Suction			No suction		
	Top of climb	Begin cruise	End cruise	Begin cruise	End cruise	Two-engine climb-out
Shaft power delivered (kW)	3768	2672	2133	3396	2791	6045
Compressor exit temperature (K)	621	577	552	663	642	700
Burner exit temperature (K)	1581	1553	1713	1513	1473	1500
Specific fuel consumption (g/kNs)	18.02	22.02	23.17	9.57	9.35	6.61
Overall efficiency	0.325	0.292	0.289	0.301	0.304	0.254

It is first notable that the design-point temperatures are below their upper limits. These values had to be imposed in order to prevent excessive burner exit temperature at end cruise. In addition, the effect of moving the design-point location in the component maps has been to reduce its efficiency relative to the ‘off-design’ conditions, thereby successfully mitigating the cruise efficiency penalty. Nonetheless, inspection of the component maps at the cruise condition reveals sub-optimal operation, especially for the high-pressure turbine. This is because the high-pressure spool runs well below its design speed when the engine is lightly

loaded.

The maximum shaft power lies between that of the T56 (3.9MW) and TP400 (8.2MW) turboprops.^e These engines have dry-weight:take-off-power ratios of 0.23kg/kW and 0.22kg/kW, respectively. Assuming a similar scaling, with 10% added for contingency, the current design is estimated to weigh 1500kg.

G. Fuel Burn

Fuel requirements are set out in Tab. 6. For the specified range of 9000km, the mission fuel weight is 27.4t, of which 1.8t (1% of take-off weight) is required to provide the potential and kinetic energy gains between take-off and cruise. Combined with the 220-passenger payload, this implies a fuel burn of 13.9g per passenger kilometer.

Table 6. LFW mission fuel breakdown

Component	Weight (kg)
Total	29,534
Mission	27,434
Reserve	1,808
Unusable	292

H. Structure and Weights

1. Structural Configuration

The passenger cabin structure is a multi-bubble arrangement, as proposed by Liebeck.²⁸ It consists of several parallel, spanwise, cylinders joined by vertical bulkheads. The bulkheads have cut-outs incorporated to allow passage throughout the cabin. Frames and stringers stabilize against potential local buckling and provide extra structural rigidity (e.g. in the event of a low-speed collision); the frames also serve to transmit local shear loads to the wing structure, in the process doubling up as wing ribs. Pressure bulkheads separate the spanwise extremes of the cabin from the unpressurized regions.²⁹ A portion of the cabin is detailed in Fig. 5.

Geuskens *et al.*²⁹ state that segregation of the cabin from the wing in this way eliminates the appearance of large pressurization stresses in the wing structure. Furthermore, with the pressure vessel supported by wing ribs, and the connections assumed pinned, it will not experience significant bending moments due to self-weight. Thus, for preliminary design purposes, the cabin and wing structures can be assumed effectively decoupled, and the cabin shell analyzed as subject to pressure loads alone.

^eInformation taken from www.rolls-royce.com/defence/products/transporters, December 2014

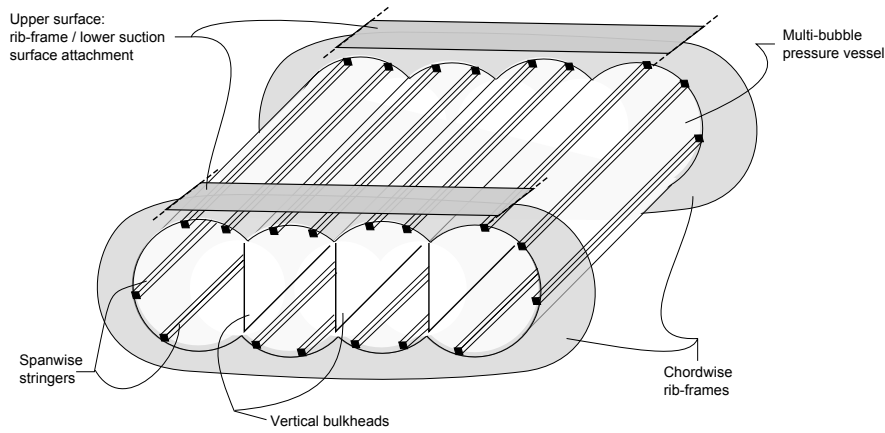


Figure 5. Passenger cabin structural arrangement.

The wing structure is conventional,³⁰ consisting of four main elements: skin, stringers, ribs and spar-webs. The suction chambers are integrated into the distributed flange construction by allowing the top of the chamber (the wing skin) and its bottom plate to resist bending loads, whilst the chamber walls act as stiffeners/stringers. Note that the porous skin thickness is set at 1mm regardless of loading, to avoid manufacturing issues.³¹

A schematic of the wing and wingtip-fin geometries is provided in Fig. 6. Four spanwise reference stations are highlighted: 1) wing root, 2) cabin boundary, 3) outboard wing/wingtip fin intersection, and 4) wingtip fin edge. The front and rear spars of the wing-box are positioned at 10% and 70% chord along the outboard regions; across the centerbody they are at a fixed distance from the nose of the aircraft, for compatibility with the cabin. The reference axis coincides with the locus of the wing-box shear center. A rectangular wing-box construction is assumed,¹⁴ with depths, selected on the basis of providing accommodation for the placement of suction equipment and structural reinforcements, of: 1) 2.3 m, 2) 2.2 m, and 3) 1.0 m.

2. Loadings

The critical in-flight load factor for passenger transports is typically the 2.5-g pull-up maneuver.¹⁴ The low wing loading of the LFW, however, means that the gust load factor is greater, at around 3.5-g (calculated following Raymer⁶). A load factor of 3-g for landing conditions is stipulated in Federal Aviation Regulation (FAR) Section 23.561.^f The internal pressurisation of the fuselage is also governed by FAR codes (Section 25.841), and is set at 0.75bar for flight altitudes above 8000ft, thereby determining the pressure difference across the cabin skin. Control surface loads are calculated for their maximum deflections. A safety factor of 1.5¹⁴ is applied to all loads.

^f<http://www.gpo.gov/fdsys/browse/collectionCfr.action?collectionCode=CFR>

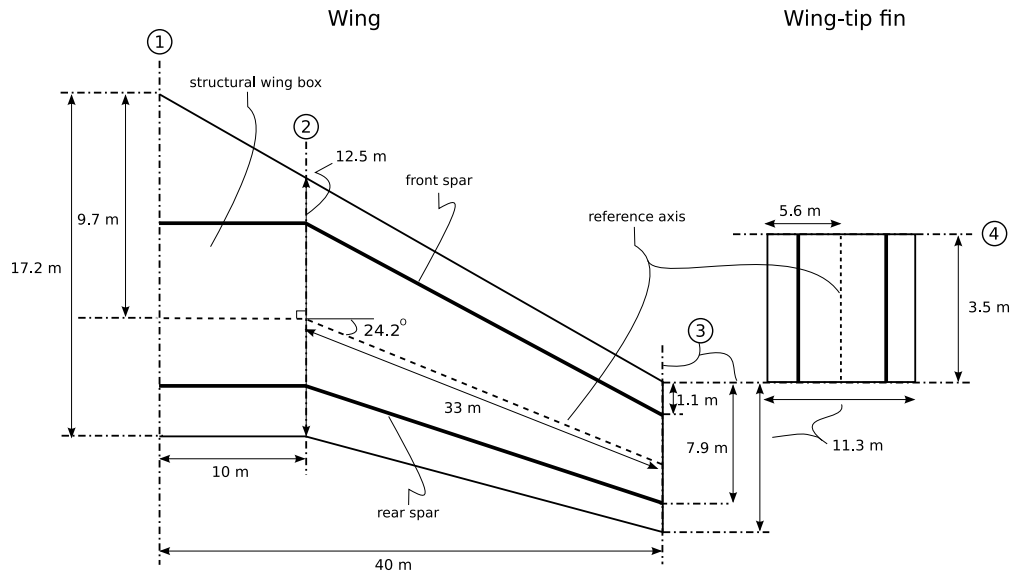


Figure 6. Wing structural geometry.

Figure 7 illustrates a) the regions over which the imposed loads act, and the critical load combinations for b) in-flight and c) on ground. Structural, payload, baggage and fuel weight are distributed between the front and rear spars; payload occupies the centerbody region, whilst baggage and fuel are placed outboard with their spanwise extent set by minimum volume requirements. (A volume per bag of 0.3m^3 and a factor of 1.5 applied to the total number of passengers gives a total baggage volume requirement of 99m^3 ; jet fuel has a density^g of around $750\text{kg}/\text{m}^3$, translating to a fuel-tank volume requirement of 40m^3 .) Baggage is placed inboard of fuel for passenger safety. The aerodynamic loading (see Sec. D) is shown as a distributed pressure force $p(y)$. The engine, auxiliary power unit (APU), suction hardware, avionics, nose wheel and undercarriage are modeled as point loads. The ground reaction force R acts as a point load through the main undercarriage location, at 75% chord on the spanwise extremes of the centerbody. The engine spacing is set at 7m. A minimum distance of 1m is reserved either side of the cabin for suction ducting.

3. Weights

The structure weight is estimated on the basis of construction with Aluminum 2024-T3. Its breakdown is provided in Tab. 7. As a fraction of the allowable aircraft weight, the 74.2t total represents around 40%, of which the wing alone accounts for 37%.

The maximum take-off weight (MTOW) consists of the payload weight, the operating empty weight (OEW), and the fuel weight. The design payload is 220 passengers (Sec. B),

^gwww.bp.com - Air BP, handbook of products.

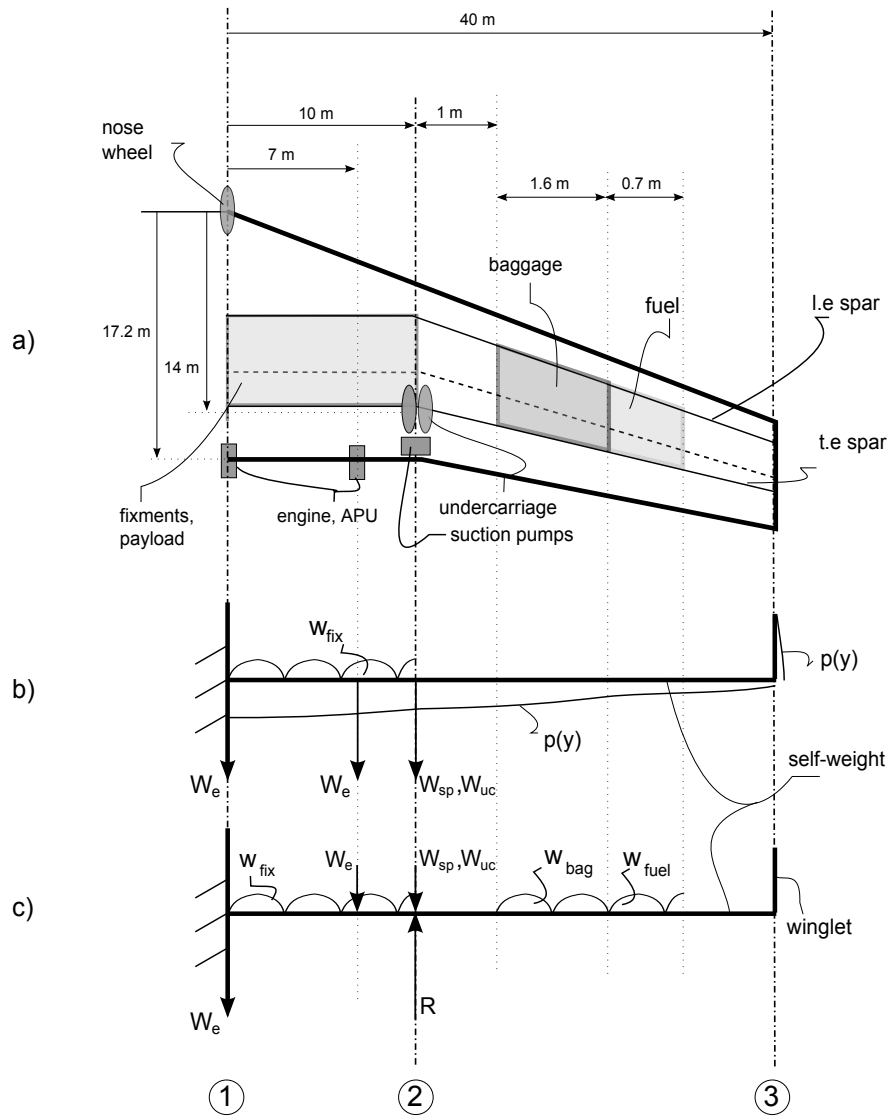


Figure 7. Distribution of weights and point loads over the planform (a), and the root cantilever model for the in-flight (b) and on-ground (c) load cases.

Table 7. LFW structural weight breakdown

Component	Wing	Component	Cabin
Flange (kg)	36,790	Skin (kg)	1,921
Stringers (kg)	19,866	Stringers (kg)	480
Shear webs (kg)	9,184	Vertical bulkheads (kg)	922
Ribs (kg)	3,899	Cabin floor (kg)	794
Control surfaces (kg)	108	Insulation (kg)	276
Total (kg)	69,847	Total (kg)	4,393

with a total weight allotment of 100kg (80kg plus 20kg of luggage) each.¹⁶ The OEW consists of contributions from the structure, propulsion system (Sec. F), suction system (Sec. E), landing gear, and fixed equipment. The landing-gear weight is estimated at 4% MTOW,¹⁶ with 10% of this allocated to the nose gear.⁶ Fixed-equipment weight consists of cabin furniture, avionics, APU, *etc.*, and is assumed equal to the payload weight;¹⁶ of the total, 10% is allocated to the avionics and 3.5% to the APU.

The aircraft weight buildup is presented in Tab. 8. The sum of the individual components is 160.6t, 26.4t below the allowable weight originally specified. In the light of the inevitable uncertainty in the structure-weight estimate for this configuration, the MTOW is set equal to the allowable weight, with the component shortfall retained as contingency. If it were required in full, the aircraft OEW would be 72%MTOW. The fuel weight with reserves is 29.5t (see Sec. G), around 16%MTOW.

Table 8. LFW aircraft weight buildup

Component	Weight (kg)
MTOW	187,000
Available weight	26,351
Design payload	22,000
Fuel with reserves	29,534
OEW	109,112
Structures	74,240
Landing gear	7,480
Fixed equipment	22,000
Propulsion	4,500
Suction pumps	895

4. Centre-of-Gravity Buildup

When the aircraft is at OEW, the C.G is furthest aft, 11.9m from the nose. Its most forward position is 11.38m, when the aircraft is at MTOW. As fuel is consumed during cruise, it moves aft to 11.44m.

The main landing gears are placed at the rear corners of the passenger cabin (see Fig. 7), 14m from the nose. This puts 15–19% of the aircraft’s weight on the nose wheel, within the range 5–20% recommended by Raymer.⁶ The gear must be long enough that the aircraft can take off and land without a wingtip strike. An overall length of 3.75m sets this limiting, ‘tip-back’, angle at 16.4°, which, in the light of a calculated maximum take-off rotation of 11.3°, should comfortably be sufficient. Then, conservatively placing the CG on the horizontal aircraft center-plane, the inclination of the CG/main-gear-wheel line to the

vertical comfortably exceeds the tipback angle. Finally, the wide wheel-base of the LFW’s undercarriage means it is in no danger of overturning while taxiing.

V. Competitor Aircraft Design

This section presents a conventional turboprop design for the same mission specification as the LFW (220 passengers, 9000 km range, cruise Mach number 0.67). With a similar payload and range, the Boeing 757-200 represents a suitable donor. Where necessary, representative dimensions, areas, weights, and loadings are obtained from figures³² for this aircraft.^h

A. Target Gross Weight

In a single-class cabin arrangement, the B757-200 has capacity of 228 passengers and an MTOW of 115,680kg. Scaling to a passenger payload of 220, the target MTOW is 111,621kg, with a wing area of 179m². Hileman *et al.*¹⁶ assume that 2%MTOW is burned by conventional aircraft in climb. This gives a start-cruise weight of 109,388kg.

B. Cruise Lift Coefficient

The optimum lift coefficient for an aircraft in cruise is given by²⁵

$$C_L = \beta \sqrt{C_{D0} \pi A_R e}. \quad (2)$$

where β is a constant parameter whose value depends on the propulsion system characteristics. Here, for the purpose of a fair comparison, it is taken to match the value derived from the LFW design (with ‘pump drag’ included in C_{D0}), 0.736. Furthermore, an Oswald efficiency, e , of 0.85 is expected to be achievable.¹⁵ It therefore remains to specify A_R and C_{D0} .

The lower flight Mach number permits reduced wing sweep. Wing-weight correlations provided by Raymer⁶ for transport aircraft show that, at some hypothetical wing weight, the sweep angle Λ may be traded for aspect ratio according to

$$A_R \propto \frac{1}{\sqrt{\cos \Lambda}}. \quad (3)$$

The B757-200 wing has 25° quarter-chord sweep and an aspect ratio of 7.8; unsweeping it according to Eq. (3) gives an aspect ratio of 9.5.

^hwww.aerospaceweb.org was also used for this purpose

van Es³³ provides an empirical method for calculating the zero-lift drag coefficient via the principle of equivalent skin friction, with a reference length formed from the aircraft wetted area and span. With the former estimated at 5.6 times wing area, the converged estimate is 0.0166.

These figures yield a design lift coefficient of 0.48, at a cruise altitude of 23,550ft. To maintain constant lift coefficient and Mach number during cruise, the aircraft must climb to 30,928ft, whilst its speed must drop from 207 m/s to 202 m/s (taking end-cruise weight equal to OEW plus payload; see Sec. G). For the associated reduction of 9% in unit Reynolds number, the change in skin-friction coefficient for a turbulent boundary along the wing is less than 2%;⁶ therefore the lift-to-drag ratio is assumed to remain constant.

C. Aircraft Geometry

Figure 8 shows the aircraft geometry in plan, side and front view. Table 9 details key parameters.

1. Fuselage

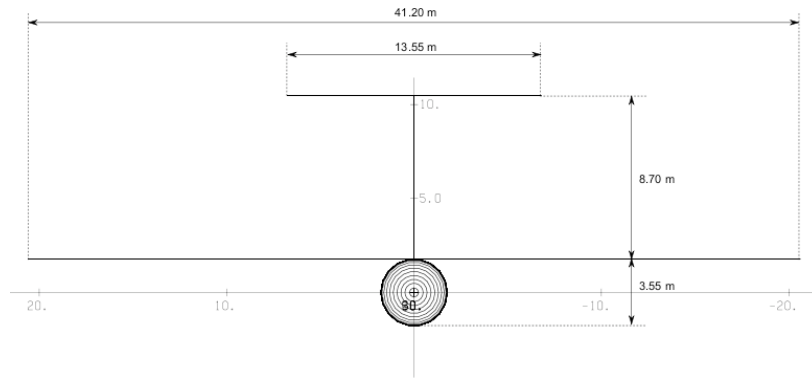
With a twin-aisle cabin, and six passengers per row, the fuselage width is 3.55m. Taking the 1m seat pitch assumed for the LFW, and the same 7m² floor area for galleys, toilets, wardrobes, *etc.*, gives a minimum cabin length of 38.7 m. The overall fuselage length is derived from the cabin length, with scale factor set by the B757-200. For simplicity, the fuselage is modeled as a cylinder with a tapered tail and elliptic nose.

2. Wing

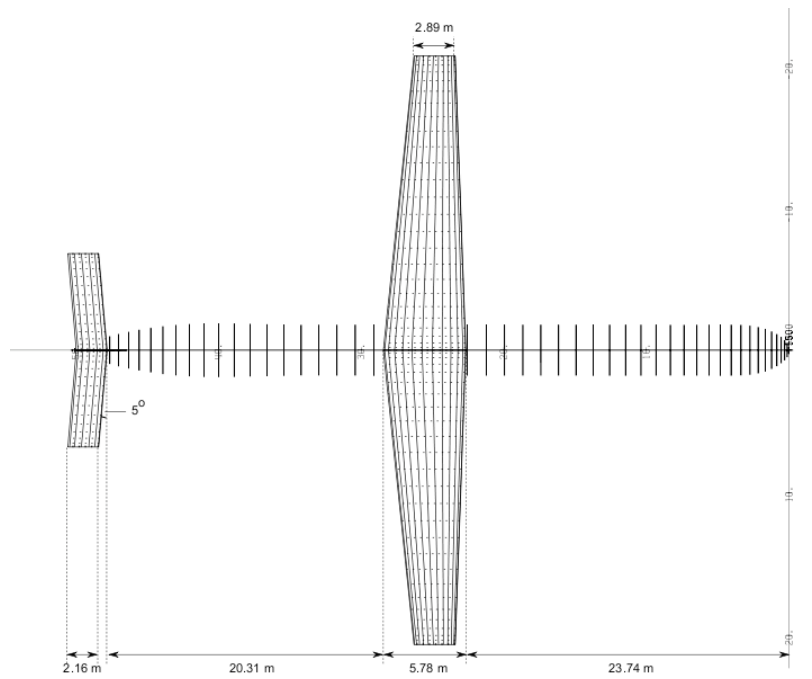
A high-mounted wing was selected to accommodate the large-diameter turboprops (see Sec. E). The taper ratio is set at 0.5, and no twist is employed. An RAE2822 airfoil with thickness-to-chord ratio 0.12 is chosen for the section, as it has been shown to exhibit satisfactory aerodynamic characteristics at transonic cruise Mach numbers.³⁴ With the quarter-chord positioned at 48% of the fuselage length, the balance and stability characteristics are satisfactory (see Sec. D).

3. Tailplane

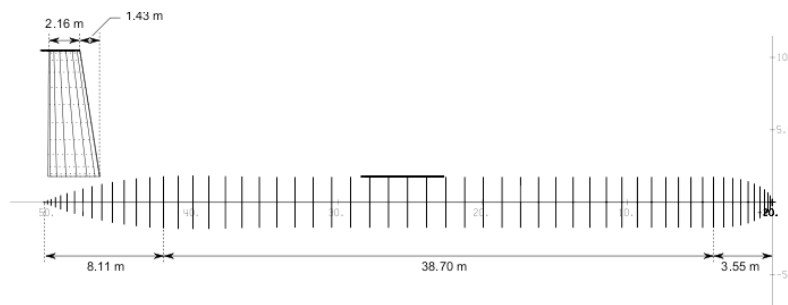
Raymer's recommendations⁶ were followed. A T-tail configuration avoids interaction between the engine efflux and the horizontal stabilizer, whose height is set so that it lies above the region of influence of the main wing when stalled. A typical taper ratio of 0.60 for the vertical fin gives it a leading-edge sweep of 9°. In contrast, the stabilizer is untapered. It



(a) Front view.



(b) Plan view.



(c) Side view.

Figure 8. Competitor aircraft configuration.

has a sweep of 5° , to avoid a stall simultaneous with the main wing at high angles of attack. Symmetrical 10% NACA-4-digit airfoils are selected for both surfaces.

Table 9. Competitor aircraft geometric parameters.

Parameter	Value
Wing area (m ²)	178.75
Wing span (m)	41.2
Wing aspect ratio	9.5
Fin area (m ²)	29.3
Stabilizer height (m)	8.7
Stabilizer area (m ²)	25
Stabilizer span (m)	13.55
Stabilizer aspect ratio	6.3

D. Performance

1. Cruise Performance

The neutral point is 25.4m from the nose. On the basis of an initial CG location estimate of 24.1m, trim is achieved with a stabilizer incidence of -1.0° and zero elevator deflection. The fuselage incidence is 2.1° , which is 0.9° below the recommended maximum.¹⁶

Figure 9 details the spanwise loading and local lift coefficient distributions. Due to the high-wing configuration, the lift distribution is not significantly affected by the presence of the fuselage. The Oswald efficiency is 0.98, significantly better than that assumed in Sec. B. The local lift coefficients correspond to fully subcritical flow on both wing and stabilizer. (Surface pressure plots are available in Ref. 5.)

The airplane viscous drag is subdivided into five groups: wing, fin and stabilizer; fuselage; engine nacelles; viscous interference; and surface discontinuities. The wing and tailplane contributions are found separately via the approach described in Sec. IIIA. The nacelle drag calculation again follows Raymer (cf. Sec. IVD1). All the other components are estimated using correlations provided by Torenbeek.¹⁵

The drag breakdown is set out in Tab. 10. The estimated lift-to-drag ratio is 18.8, which is representative of conventional configurations.²⁴

2. Low-Speed Performance

Torenbeek¹⁵ states that the drag polar on initial climb-out can be approximated by the standard quadratic form

$$C_D = C_{D0} + \frac{C_L^2}{\pi A Re}, \quad (4)$$

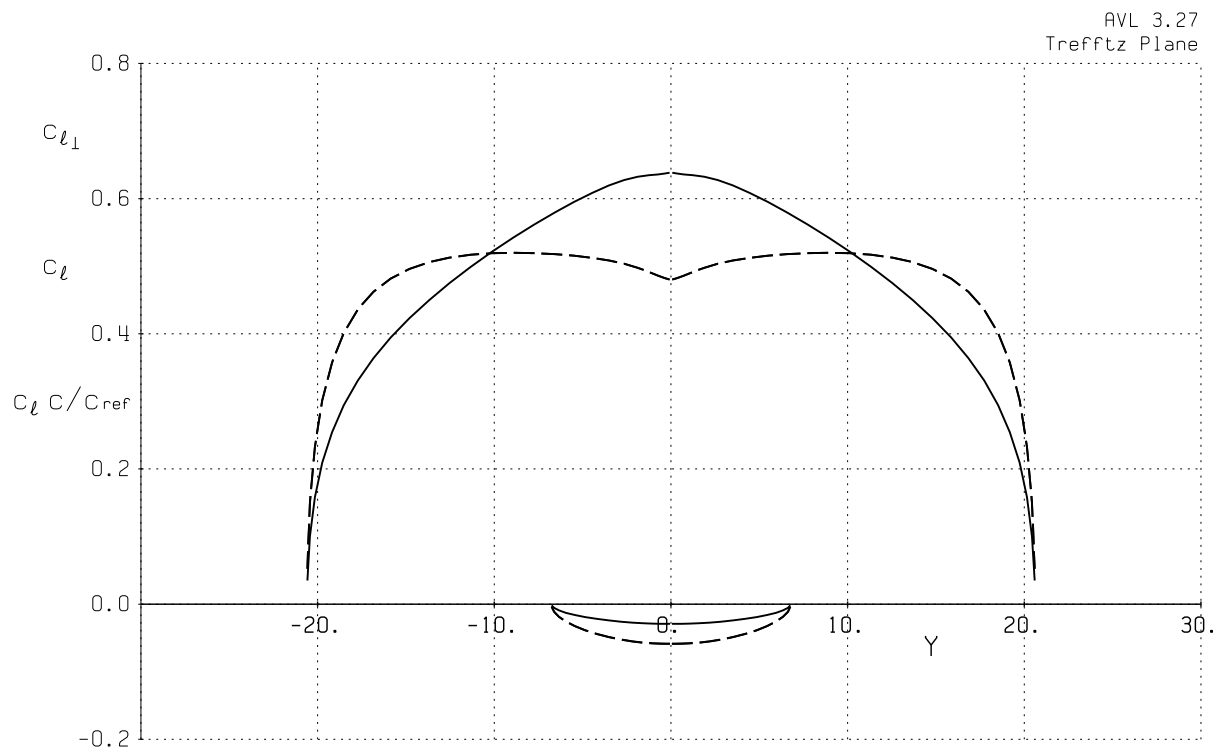


Figure 9. Spanwise loading distributions for $C_L = 0.48$ and $M_\infty = 0.67$: C_l (dashed) and $C_l c / c_{ref}$ (solid). Positive values are for the wing, negative for the tailplane.

Table 10. Competitor aircraft cruise drag coefficients.

Coefficient	Value
C_L	0.48
C_D	0.0256
C_{D_i} (e)	0.0079 (0.980)
C_{D_v} wing	0.0066
C_{D_v} vertical fin	0.0011
C_{D_v} stabilizer	0.0012
C_{D_v} fuselage	0.0068
C_{D_v} engine nacelles	0.0014
C_{D_v} interference effects	0.0002
C_{D_v} surface discontinuities	0.0004

but with $C_{D0} = 0.018$ and $e = 0.672$. At an initial climb-out speed of 70 m/s, $C_L = 2.04$. The lift-to-drag ratio was thus found to be around 9.

E. Propulsion System

As for the LFW, a two-spool turboprop architecture was specified. However, the design point reverted to the conventional, top-of-climb, condition.

1. Thrust and Power Requirements

Two engines sized to meet conditions at top-of-climb were unable to meet climb-out thrust requirements without excessive burner exit temperatures. Therefore, a four-engine configuration was adopted. The requirements per engine are summarized in Tab. 11. Climb-out thrust is based on a minimum flight-path angle of 1.72° with one engine inoperative;²⁵ the top-of-climb and cruise angles are 0.5° and 0° , respectively (as in Sec. IVF). The auxiliary power off-take is set so that the total, 150kW, matches that of the LFW.

Table 11. Thrust and power off-take requirements (per engine) for the competitor aircraft.

Parameter	Top of climb	Begin cruise	End cruise	Three-engine climb-out
Altitude (m)	7178	7178	9427	120
Mach number	0.67	0.67	0.67	0.21
Thrust (kN)	16.6	14.3	10.5	51.3
Power off-take (kW)	37.5	37.5	37.5	37.5

2. Engine Performance

Design-point parameters were set as follows: compressor and burner exit temperature limits 700K and 1800K respectively; propellor diameter 4.3m; propellor speed 1100RPM. The engine performance is summarized in Tab. 12. The specific fuel consumption figures are significantly better than those of the LFW (see Tab. 5), but, as explained in Sec. IVF3, the overall efficiency parameter is a more suitable measure in the context of significant power off-take. This, too, is superior, at about 37% in cruise, compared with 29% for the LFW. Finally, the design compromises that gave the LFW engine a notably higher efficiency at top-of-climb than in cruise are absent here; hence the competitor aircraft values are barely distinguishable.

Table 12. Competitor aircraft engine performance.

Parameter	Top of climb	Begin cruise	End cruise	Three-engine climb-out
Shaft power delivered (kW)	3998	3444	2454	5344
Compressor exit temperature (K)	700	676	641	715
Burner exit temperature (K)	1800	1726	1664	1798
Specific fuel consumption (g/kNs)	13.1	13.3	12.8	6.5
Overall efficiency	0.374	0.369	0.373	0.256

The maximum shaft power occurs on climb-out, and has a value of 5344kW. Based on this parameter (see Sec. IVF3), the engine weight is 1.26t.

F. Fuel Burn

The calculated mission, reserve and unusable fuel weights are given in Tab. 13. The mission fuel requirement is 28.8t, of which 0.6t (0.6%MTOW) is to provide the potential and kinetic energy increases between take-off and cruise. The consumption per passenger is 14.6g/km.

Table 13. Competitor fuel weight breakdown.

Fuel	Mass (kg)
Total	31,609
Mission	28,827
Reserve	2470
Unusable	316

G. Structure and Weights

1. Structural Weight

A 2.5-g pull-up maneuver in cruise flight is taken as the critical loading condition for the wing. System loads acting on each wing consist of two engines mounted on the leading edge at 24% and 66% half-span. Fuel weight acts to provide bending relief, and is (conservatively) not included in the calculation. The total estimated wing weight is 15.3t, which is around 14%MTOW; a breakdown is provided in Ref. 5.

Typically, a pull-out maneuver in a nose dive is critical for the horizontal stabilizer;¹⁴ for this case, the lift distribution on the tailplane in trimmed cruise is scaled up to its maximum section C_l of 0.80.³⁵ The vertical fin is sized to react loads incurred during three-engine climb-out, and is scaled by a factor of 0.70 to account for inertial effects.¹² The total tailplane weight is 1.6t, which is less than 2%MTOW.

The fuselage shell, tail cone, floor and added bending material are sized to withstand the following applied loadings: differential pressure; horizontal and vertical bending moments in flight and on landing; and torsional shear.¹² The remainder of the fuselage weights are estimated using empirical correlations provided by Torenbeek¹⁵ for: shell modifications, consisting of added weights including rivets, fasteners, local reinforcements, *etc.*; and the support structures of the wing, tailplane and fuselage-mounted landing gear. The total fuselage weight estimate is 10.0t, around 9%MTOW; its breakdown is given in Ref. 5.

The overall structural weight is calculated at 26.9t, as shown in Tab. 14. The wing, tail and body structures account for 57%, 6% and 37%, respectively; for comparison, the corresponding figures for the B737-200 areⁱ 43%, 11% and 46%.

Table 14. Competitor aircraft structural weight breakdown.

Component	Mass (kg)	% total
Wing	15,287	56.8
Tailplane	1597	5.9
Fuselage	10,024	37.3
Total	26,908	

2. Aircraft Weight Buildup and Centre-of-Gravity Travel

The aircraft weight buildup is presented in Tab. 15. The OEW contributes 52%MTOW, a figure which compares well with conventional aircraft configurations. (The Boeing 757-200, for example, has an empty-weight fraction of 0.55.³²) Fuel with reserves represents

ⁱ<http://adg.stanford.edu/aa241/AircraftDesign.html>

28%MTOW.

Table 15. Competitor aircraft weight buildup.

Component	Mass (kg)
MTOW	112,006
OEW	58,397
Design payload	22,000
Fuel with reserves	31,609
Structure	26,908
Fixed equipment	22,000
Landing gear	4,465
Propulsion	5,024

Compared to the initial design target, 111,621kg, the MTOW is 0.3% higher, a discrepancy which is negligible at the level of this analysis. Therefore no iteration was undertaken.

The furthest aft CG location is at 25.1m, when the aircraft is loaded with fuel only. In contrast, the foremost location, at 23.9m, corresponds to full payload and no fuel. The mean CG position during cruise is 24.35 m, which is 0.25m aft of that assumed for the pitch trim analysis.

VI. Discussion

The design analysis has yielded fuel consumption estimates of 13.9g and 14.6g per passenger kilometer for the LFW and the competitor aircraft respectively. Given the LFW's manifestly superior aerodynamic efficiency, these figures demand explanation. Further insight can be obtained by considering the simplified (Breguet) range equation,¹⁵ which can be written to give the following explicit expression for the payload fuel efficiency:

$$\frac{W_f}{XW_p} = \frac{1}{X} \left(1 + \frac{W_e}{W_p} \right) \left[\exp \left(\frac{X}{(H_0/g)\eta(L/D)} \right) - 1 \right]. \quad (5)$$

This form highlights the rôle of the empty-to-payload weight ratio, W_e/W_p , and it is this parameter which handicaps the LFW. Despite having a much better combined engine and aerodynamic efficiency, $\eta L/D$, than the competitor (17.8 compared to 7.0), it shows little overall improvement because it has $1 + W_e/W_p = 7.16$, almost twice the competitor's 3.65.

The LFW figure is conservative, though, since it assumes that the calculated empty weight of 109t has been augmented by the 26t left available for contingencies. If none of this were required, then the fuel consumption would scale (approximately) in proportion to the overall weight reduction, dropping to 11.9g per passenger kilometer. Nonetheless,

this figure remains well above Green’s¹ LFW fuel-consumption estimates, which translate to per-passenger figures of 7.2g/km and 6.3g/km, for turbofan and unducted-fan propulsion respectively. All other factors being equal, one would expect a turboprop-powered LFW to lie between these values. The explanation for the discrepancy again lies in the weight ratio. Green’s designs have lift-to-drag ratio 37, and engine efficiencies of 0.37 and 0.42, giving somewhat *less* favorable estimates of $\eta L/D$ than obtained here, but they have a markedly lower empty-to-payload weight fraction (2.4, compared to 5.0 for the current design without contingency weight).

The other shortfall in the current design is engine efficiency. If this parameter could be brought up to the level achieved for the competitor aircraft, then the LFW’s fuel consumption advantage would become more significant. Although there is a good reason for the low value — the extreme thrust range demanded of the engine makes its design unusually difficult — performance would be improved by allowing the aircraft to cruise higher (at the same Mach number). Assuming, as a first approximation, that the zero-lift drag remains constant, the lift-to-drag ratio also improves initially, and is only marginally degraded (to 60.5) when cruise is at 30,000ft, with lift coefficient 0.19. Assuming also (conservatively, in the light of its general parametric dependence⁹) that the suction power requirement is unchanged, further engine calculations show that this point marks the peak value of $\eta L/D$, 18.8. Not all of this gain would be available, however, since the cabin weight would also rise. Assuming a linear increase with the pressure differential adds 1565kg to the aircraft empty weight, in which case the fuel-consumption estimate becomes 11.4g per passenger kilometer.

In summary, the concept presented here does not achieve the remarkable advance over the conventional configuration expected of the LFW. It can, however, be regarded as representing a boundary for the available design space; one where emphasis is placed solely on aerodynamic efficiency. In the light of its weight-ratio and thrust-discrepancy problems, it seems likely that an optimum configuration will be found at lower aspect ratio and higher sweepback. In any case, recognition of these design conflicts is a prerequisite for future studies.

VII. Conclusion

This paper has presented a design study of an LFW passenger aircraft, with a specification — 80m span, 20% thickness-to-chord ratio, Mach 0.67 cruise — chosen to exploit this configuration’s potential aerodynamic efficiency advantage to the full. As a result, the 161–187t design has a lift-to-drag ratio of 60.9. Powered by three turboprop engines, it carries 220 passengers over a range of 9000km, at a fuel consumption of 11.4–13.9g per passenger kilometer. These figures represent a considerable improvement over current aircraft;

nonetheless, they are roughly double Green's¹ preliminary estimates for the type.

For comparison purposes, a competitor aircraft, with the same mission, has also been designed. This 112t vehicle has a conventional configuration, with a straight wing and four turboprop engines. Its lift-to-drag ratio of 18.8 is comparable to current aircraft, but its estimated fuel consumption — 14.6g per passenger kilometer — is again better, due to the use of turboprops.

Thus, despite its spectacular lift-to-drag ratio, the current LFW concept holds only a slender advantage over the competitor design. This is because its engine efficiency and empty-to-payload weight ratio are markedly worse. Both issues are fundamental to the current specification. The engine efficiency is degraded because of design compromises imposed by the huge difference in required thrust between (engine-out) climb-out and low-drag cruise. The high weight ratio is a by-product of the low wing loading and large span necessary to bring induced drag down to a level comparable to the viscous component. It can be concluded that an optimized LFW design would have to sacrifice aerodynamic efficiency to mitigate these problems. This conflict may limit the extent to which Green's predictions are achievable.

Acknowledgments

This paper has benefited from the perceptive comments made by its reviewers, especially with regard to the influence of altitude on engine efficiency. The first author thanks the Engineering and Physical Sciences Research Council (EPSRC) for financial support via its 'Doctoral Training' scheme. Supporting research data is available at:

<https://www.repository.cam.ac.uk/handle/1810/247199/browse?type=title>

References

¹Green, J. E., "Greener by Design: The Technology Challenge," *The Aeronautical Journal*, Vol. 106, No. 1056, 2002, pp. 57–113.

²Martinez-Val, R., Perez, E., Alfaro, P., and Perez, J., "Conceptual Design of a Medium Size Flying Wing," *Proc. IMechE Part G: J. Aerospace Engineering*, Vol. 221, No. 1, 2007, pp. 57–66.

³A. L. Braslow & M. C. Fischer, "Design Considerations for Application of Laminar Flow Control Systems to Transport Aircraft," *Aircraft Drag Prediction and Reduction*, AGARD Report R-723, 1985.

⁴R. D. Joslin, "Aircraft Laminar Flow Control", *Annu. Rev. Fluid Mech.*, Vol. 30, 1998, pp. 1–29.

⁵Saeed, T. I., "Conceptual Design for a Laminar-Flying-Wing Aircraft," Ph.D. Dissertation, Univ. of Cambridge, Cambridge, 2012. uri: <http://www.dspace.cam.ac.uk/handle/1810/243926>

⁶Raymer, D. P., *Aircraft Design: A Conceptual Approach*, 4th ed., AIAA Education Series, AIAA, Reston, VA, 2006.

⁷Ashill, P. R., Wood, R. F., and Weeks, D. J., “An Improved, Semi-Inverse Version of the Viscous Garabedian and Korn Method (VGK),” Royal Aircraft Establishment Tech. Rep. 87002, 1987.

⁸Eppler, R., and Somers, D. M., “A Computer Program for the Design and Analysis of Low-Speed Airfoils,” NASA TM-80210, 1980.

⁹Saeed, T. I., Graham, W. R., and Hall, C. A., “Boundary-Layer Suction System Design for Laminar-Flying-Wing Aircraft,” *Journal of Aircraft*, Vol. 48, No. 4, 2011, pp. 1368–1379. doi: 10.2514/1.C031283

¹⁰Drela, M., “XFOIL: An Analysis and Design System for Low Reynolds Number Airfoils,” *Lecture Notes in Engineering* Vol. 54, Proceedings of the Low Reynolds Number Aerodynamics Conference, Notre Dame, edited by T. J. Mueller, Springer, Berlin, 1989, pp. 1–12.

¹¹Young, A. D., *Boundary Layers*, BSP Professional Books, Oxford, 1989.

¹²Greitzer, E. M., *et al.*, “N+3 Aircraft Concept Designs and Trade Studies, Final Report/Appendix,” NASA CR-2010-216794/Vol. 1/Vol. 2, 2010.

¹³Ardema, M. D., Chambers, M. C., Patron, A. P., Hahn, A. S., Miura, H., and Moore, M. D., “Analytical Fuselage and Wing Weight Estimation of Transport Aircraft,” NASA TM-110392, 1996.

¹⁴Howe, D., *Aircraft Loading and Structural Layout*, Professional Engineering Publishing Ltd., London, 2004.

¹⁵Torenbeek, E., *Synthesis of Subsonic Airplane Design*, Kluwer Academic Publishers, Dordrecht, 1982.

¹⁶Hileman, J. I., Spakovsky, Z. S., Drela, M., Sargeant, M. A., and Jones, A., “Airframe Design for Silent Fuel-Efficient Aircraft,” *Journal of Aircraft*, Vol. 47, No. 3, 2010, pp. 956–969. doi: 10.2514/1.46545

¹⁷Pratt, R. W., *Flight Control Systems: Practical Issues in Design and Implementation*, Institution of Engineering and Technology, London, 2000.

¹⁸Cook, M., *Flight Dynamics Principles*, Arnold, London, 1997.

¹⁹Nickel, K., and Wohlfart, M., *Tailless Aircraft in Theory and Practice*, Butterworth-Heinemann, Oxford, 1994.

²⁰Northrop, J. K., “The Development of All-Wing Aircraft,” *Journal of the Royal Aeronautical Society*, Vol. 51, 1947, pp. 481–510.

²¹Donlan, C. J., “An Interim Report on the Stability and Control of Tailless Airplanes,” NACA Report No. 796, 1944.

²²Nelson, R. C., *Flight Stability and Automatic Control*, McGraw-Hill, Boston, MA, 1998.

²³Bolsunovsky, A. L., *et al.*, “Flying Wing — Problems and Decisions,” *Aircraft Design*, Vol. 4, No. 4, 2001, pp. 193–219.

²⁴Cumpsty, N. A., *Jet Propulsion*, Cambridge University Press, Cambridge, 1997.

²⁵Mair, W. A., and Birdsall, D. L., *Aircraft Performance*, Cambridge University Press, Cambridge, 1992.

²⁶Wilson, R. A. L., “The Introduction of Laminar Flow to the Design and Optimisation of Transport Aircraft,” Ph.D. Dissertation, Cranfield Univ., Cranfield, 1997.

²⁷Mitchell, G. A., “Experimental Aerodynamic Performance of Advanced 40°-Swept, 10-Blade Propeller Model at Mach 0.6 to 0.85,” NASA TM-88969, 1988.

²⁸Liebeck, R. H., “Design of the Blended Wing Body Subsonic Transport,” *Journal of Aircraft*, Vol. 41, No. 1, 2004, pp. 10–25. doi: 10.2514/1.9084

²⁹Geuskens, F. J. J. M. M., “Non-Cylindrical Pressure Fuselages for Future Aircraft,” AIAA Paper 2008-1907, 2008.

³⁰Niu, M. C., *Airframe Structural Design*, Conmilit Press Ltd., Hong Kong, 1988.

³¹Inger, G. R., and Babinsky, H., “Viscous Compressible Flow Across a Hole in a Plate,” *Journal of Aircraft*, Vol. 37, No. 6, 2002, pp. 1028–1032. doi: 10.2514/2.2707

³²Aboulafia, R., *Jane’s Civil Aircraft*, Harper Collins, London, 1996.

³³van Es., G. W. H., “Rapid Estimation of the Zero-Lift Drag Coefficient of Transport Aircraft,” *Journal of Aircraft*, Vol. 39, No. 4, 2002, pp. 597–599. doi: 10.2514/2.2997

³⁴Drela., M., and Giles, M. B., “Viscous-Inviscid Analysis of Transonic and Low Reynolds Number Airfoils”, *AIAA Journal*, Vol. 25, No. 10, 1986, pp. 1347–1355. doi: 10.2514/3.9789

³⁵Polentz, P. P., “Comparison of the aerodynamic characteristics of the NACA0010 and 0010-64 airfoil sections at high subsonic Mach numbers,” NACA RM-A9G19, 1949.